# Effect of microcirculatory resistance on coronary blood flow and instantaneous wave-free ratio: A computational study

Liu, H., Ou, S., Liu, P., Xu, Y., Gong, Y., Xia, L., Leng, X., Leung, T. W. H., Shi, L. & Zheng, D.



**Original citation & hyperlink:**
Liu, H, Ou, S, Liu, P, Xu, Y, Gong, Y, Xia, L, Leng, X, Leung, TWH, Shi, L & Zheng, D 2020, 'Effect of microcirculatory resistance on coronary blood flow and instantaneous wave-free ratio: A computational study', Computer Methods and Programs in Biomedicine, vol. 196, 105632. https://dx.doi.org/10.1016/j.cmpb.2020.105632

DOI 10.1016/j.cmpb.2020.105632
ISSN 0169-2607

Publisher: Elsevier

**Effect of microcirculation resistance on coronary blood flow and instantaneous wave-free ratio: a computational study**

**Haipeng Liu[1], Shanxing Ou[2], Panli Liu[3], Yuhang Xu[1], Yinglan Gong[4], Ling Xia[4], Xinyi Leng[5], Thomas Wai Hong Leung[5], Lin Shi[6*], Dingchang Zheng[1*]**

[1] Research Centre of Intelligent Healthcare, Faculty of Health and Life Science, Coventry University, Coventry CV1 5FB, UK
[2] Department of radiology, General Hospital of Southern Theater Command, PLA, Guangzhou, China
[3] Department of radiology, Guangzhou First People's Hospital, Nansha Hospital, Guangzhou, China
[4] Department of Biomedical Engineering, Zhejiang University, Hangzhou, China
[5] Department of Department of Medicine and Therapeutics, The Chinese University of Hong Kong, Prince of Wales Hospital, Shatin, Hong Kong, China
[6] Department of Imaging and Interventional Radiology, The Chinese University of Hong Kong, Prince of Wales Hospital, Shatin, Hong Kong, China

***Corresponding authors**

## Abstract

**Background and Objective:** The instantaneous wave-free ratio (iFR) has been proposed to estimate the hemodynamic severity of atherosclerotic stenosis in coronary arteries. The atherosclerotic stenosis in a proximal coronary artery could change its distal microcirculatory resistance (MR). However, there is a lack of investigation about the effect of MR variation on the blood flow and iFR of stenotic coronary arteries. We aim to investigate the changes of blood flow and iFR caused by distal MR variation.

**Methods:** Four three-dimensional models of coronary arteries were reconstructed from the computed tomography images of two normal cases and two cases with 74.9% and 96.4% (in area) stenoses in a large branch of left anterior descending artery (LAD). Computational fluid dynamics simulation was performed on each model under 6 MR variations: hyperemia as the reference situation, resting when MR was multiplied by 8/3 in all outlet branches, h-one-1.5 and h-one-2 when MR was multiplied by 1.5 and 2.0 in one branch (the stenotic, or the corresponding branch in normal case) of LAD, h-branches-1.5 and h-branches-2 when MR was multiplied by 1.5 and 2.0 in the stenotic/corresponding and its cognate branches. Flow rate and iFR of each outlet branch were then calculated and compared between different MR situations to investigate the effect of MR variation on flow rate and iFR.

**Results:** In 74.9% stenosed and normal cases, referring to the hyperemia situation, the increase of MR in any branch significantly decreased its flow rate and increased its iFR, with limited effect on the flow rate (<3%) and iFR (<0.01) of other branches. However, in the 96.4% stenosed case, the doubled MR in the stenosed branch (h-one-2) significantly increased the flow rate (>10%) and iFR (>0.05) of its cognate branches.

**Conclusion:** The increase of MR in a normal or mildly stenosed branch of coronary artery decreases its blood flow and increases its iFR, with limited effect on other branches. Whereas, the increase of MR in a severely stenotic large branch could significantly increase the flow velocity and iFR of its cognate branches.

**Key words:** coronary microvascular dysfunction (CMD); instantaneous wave-free ratio (iFR); computational fluid dynamics (CFD)

## 1. Introduction

Atherosclerotic stenosis decreases the blood flow in coronary arteries, resulting in angina and acute myocardial infarction. It has been reported that the luminal severity of stenosis does not reflect the hemodynamic severity of blood flow reduction and thus is insufficient to guide therapy (with sensitivity<85%, Specificity<65%) (1). Currently, fractional flow reserve (FFR), defined as the ratio between hyperemic and resting arterial blood flow rates, is considered to be the gold standard for assessing the hemodynamic significance of stenoses in coronary arteries, where FFR>0.9 and FFR<0.8 indicate normal and severely stenotic coronary arteries, respectively (2). In clinical practice, FFR is simplified as the hyperemic ratio between distal-to-stenosis and aortic pressures.

The diagnostic accuracy of FFR has been reported to be affected by the microcirculatory (or microvascular) resistance (MR) (3). The blood flow in an artery is related positively to the inlet blood pressure and negatively to the flow resistance. In coronary arteries, MR of the arterioles and capillaries accounts for more than 80% of the total flow resistance (4). Due to the effect of myocardial contraction on arterioles and capillaries, the ratio between maximum and minimum MR values in a cardiac cycle is

larger than 6, resulting in FFR variation larger than 0.2 (5). Accordingly, the instantaneous wave-free ratio (iFR) has been proposed as a promising substitute of FFR (6). The iFR is defined as the ratio between distal-to-stenosis and aortic pressures measured during the wave-free period. The wave-free period extends from the end of first 25% period of diastole to 5 ms before the end of diastole, when MR is stable and minimized (6). The iFR could minimize the effect of periodic MR fluctuation on the estimation of arterial blood flow (7), and showed a good agreement (>60%) with the quantitative flow ratio derived from in vivo measurements in classifying the nonculprit coronary lesions (8).

MR changes pathologically due to the atherosclerotic stenosis in proximal coronary arteries (4). In some chronic cardiac diseases, because of the thickened small intramural arteries with narrowed lumens, hyperemic MR could increase by 40% (9). A clinical study has shown that iFR remains stable irrespective of the changes in MR (10). However, another study on FFR has indicated that the abnormal hyperemic MR may affect the diagnostic reliability when using iFR (11). Therefore, the effect of MR on iFR needs further investigation before achieving diagnostic application.

Computational fluid dynamics (CFD) has been widely used for simulating blood flow in coronary arteries. Combined with cardiovascular imaging, CFD simulation enables detailed characterization of flow fields and the computation of hemodynamic parameters which are difficult to be directly measured such as pressure, flow velocity, and FFR (12). A growing body of evidence has validated the diagnostic accuracy of CFD-derived FFR compared with invasive FFR (13). Furthermore, it has been reported that the iFR values derived from CFD simulation were consistent with in-vivo measured FFR (6). However, to the best of our knowledge, there is no CFD study investigating the effect of physiological and pathological variations of MR on iFR and blood flow velocity in coronary arteries with atherosclerotic stenosis. In this study, the effect of MR on iFR and blood flow velocity in normal and stenotic coronary arteries will be comprehensively investigated.

## 2. Methods

### 2.1. Geometric model reconstruction from imaging data

In this computational study, the geometric models for CFD simulation were reconstructed from the computed tomography (CT) imaging data of two male patients with coronary stenosis and two normal controls (one male and one female). The imaging data were collected in General Hospital of Guangzhou Military Command of PLA from 2015 to 2016 with approval from the local ethics committee. Individuals were well informed with consent form signed.

The three-dimensional (3-D) models of left coronary arteries were reconstructed from the CT images using the software MIMICS 18.0 (Materialise N.V., Belgium). The 3-D geometric models started from the inlet of left main coronary artery (LMCA) on the aorta and extended to the distal branches of left anterior descending artery (LAD) and left circumflex artery (LCX), with small branches (diameter<1mm, or blurred structure) trimmed off. The geometry was smoothed with errors (self-intersections, spikes, small holes, etc.) amended in software Geomagic Studio 12.0 (3D Systems, Rock Hill, South Carolina, USA). Finally, the inlet and outlets were sectioned vertically to the local arterial centerlines.

Figure 1 shows the reconstructed 3-D models (2 stenotic arterial models and 2 normal controls). The stenosis located in a major branch of LAD in Case 1 and Case 3 (branch 1 in Fig.1). The four cases were coupled into two groups according to the number of their outlets. The first and second models (Case 1 and Case 2) were stenotic and normal control cases, respectively, and each model contained 6 outlets. Similarly, the third and fourth models (Case 3 and Case 4) were stenotic and normal cases,

respectively, with 11 outlets. The coupled patient-specific models enabled us to comprehensively investigate the effect of MR variation on blood flow and iFR in normal and stenotic coronary arteries.

For each stenosis, the diameter severity (DS) and area severity (AS) were defined as $DS = 1\text{-}\frac{\text{diameter at stenotic throat}}{\text{normal diameter}}$ and $AS = 1\text{-}\frac{\text{cross-sectional area at stenotic throat}}{\text{normal cross-sectional area}}$. Case 1 had a mild stenosis (DS: 46.5%, AS: 74.9%) while Case 3 had a more severe stenosis (DS: 73.8%, AS: 96.4%).

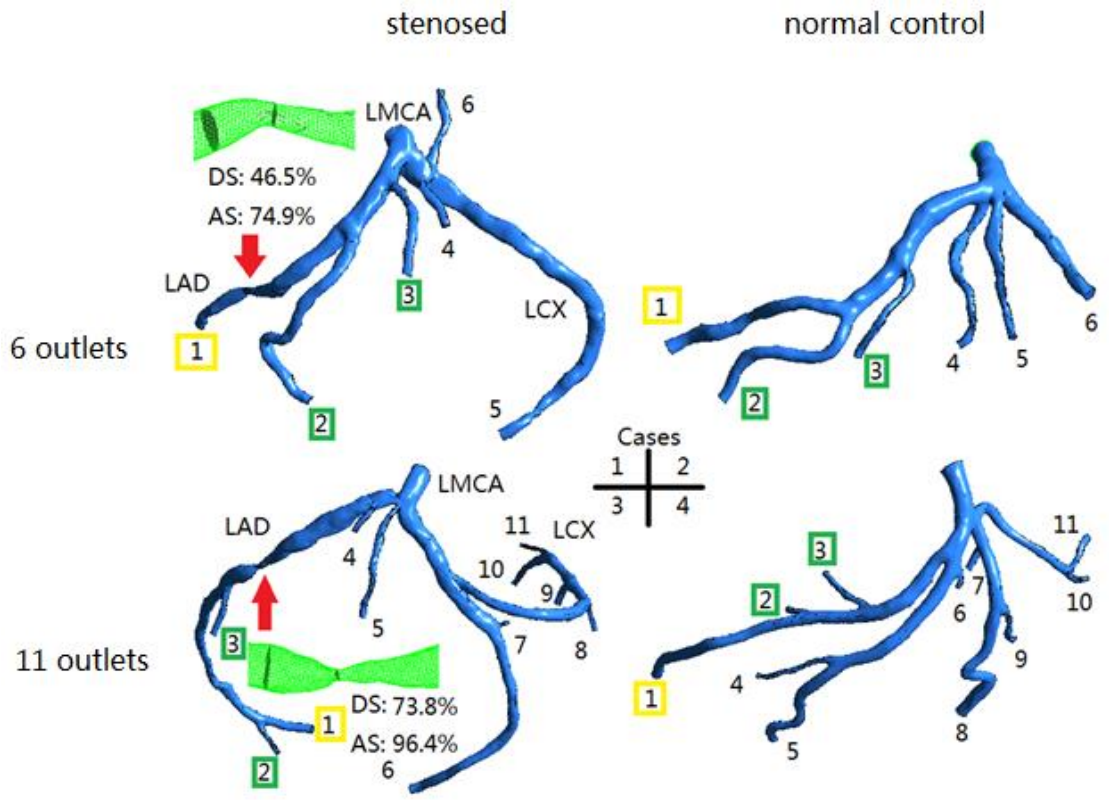


Figure 1. 3-D models of coronary arteries reconstructed from CT images. Cases 1 and 3 have mild and severe stenoses in left anterior descending artery (LAD), with cases 2 and 4 as normal controls. Cases 1 and 2 have 6 outlets, while cases 3 and 4 have 11 outlets. Yellow rectangles indicate the largest branch distal to the stenotic segment, with green rectangles indicating its cognate branches (and their counterparts in corresponding normal cases). LMCA: left main coronary artery. LAD: left anterior descending artery. LCX: left circumflex artery. DS: diameter severity. AS: area severity.

**2.2. CFD modeling of MR variation**

The geometric models were input into the software ANSYS ICEM-CFX-15.0 (ANSYS, Inc., Canonsburg, PA) for meshing and CFD simulation. Tetrahedron elements were used for meshing. The maximum element length was 0.25mm globally and 0.1mm at inlet and outlets. We have performed the mesh density dependence study in our published work in which the maximum element length of 1mm at the vessel wall and 0.2mm at coronary artery outlet has been proven to be reliable for the simulation of trans-stenotic pressure drop and FFR (14).

The fluid domain was modeled using the incompressible, steady, and Newtonian Navier–Stokes equations: $\begin{cases} \nabla \cdot \vec{u} = 0 \\ \rho\left(\frac{\partial \vec{u}}{\partial t} + \vec{u} \cdot \nabla \vec{u}\right) + \nabla p - \mu \nabla^2 \vec{u} = 0 \end{cases}$, where $\rho$ is the fluid density (1060kg/m^3),

$\mu$ is the fluid viscosity. $\vec{u}$ and $p$ are the fluid velocity and pressure respectively. The laminar flow assumption was used as in the existing study on CFD simulation of stenosed coronary arteries (15). Although blood is essentially a non-Newtonian fluid due to its shear-thinning effect, the rheological influence on pressure and flow rate is negligible (14). Therefore, in this study, blood was modeled as a Newtonian fluid with a constant viscosity of 0.0035Pa.s.

Boundary condition and simulation: The diastolic aortic blood pressure of 80mmHg was applied at the inlet of LMCA. In vivo measurement showed that the diastolic aortic blood pressure is 77.9 ± 12.9 mmHg (mean ± SD) (16). The non-slip and solid wall assumption was used. MR was applied as outlet condition. Six situations of MR (hyperemia, resting, h-one-1.5, h-branches-1.5, h-one-2, h-branches-2) were simulated:

- The reference "hyperemia" situation was simulated by distributing the normal hyperemic MR value of left coronary artery to all outlet branches according to the modified Murray's law: $\frac{Q_1}{Q_2} = \left(\frac{D_1}{D_2}\right)^{\frac{7}{3}}$, where Q1 and Q2 are the flow rates, while D1 and D2 are the diameters of two distal branches at a bifurcation (17).
- The "resting" situation was simulated by multiplying normal hyperemic MR values of all outlets by 8/3, which is approximating to the averaged value in adults with FFR>0.5 (18).
- In the "h-one-1.5" situation, the mild MR increase (multiplying normal hyperemic MR by 1.5) was applied to the stenotic branch (or its counterpart in corresponding normal model) of LAD (outlets with yellow rectangles in Fig.1).
- In the "h-branches-1.5" situation, mild MR increase (multiplying normal hyperemic MR by 1.5) was applied to the stenotic branch and all its cognate branches, or their counterparts in corresponding normal cases (outlets with green and yellow rectangles in Fig.1).
- The severe MR increase ("h-one-2" and "h-branches-2", multiplying normal hyperemic MR by 2) was simulated similarly as in "h-one-1.5" and "h-branches-1.5".

In all CFD simulations, the convergence criterion was 1.0E-4.

**2.3. Hemodynamic parameters: flow rate and iFR**

For each outlet branch, the flow rate was quantified as the area-averaged flow velocity on the cross-section of outlet. The iFR was measured during the wave-free period in diastole as $iFR = \left.\frac{P_d}{P_a}\right|_{\text{wave-free period}}$, where Pa and Pd are aortic and distal-to-stenosis pressures, simplified as the area-averaged pressure values of inlet and outlet.

**2.4. Model validation: hyperemic flow velocity**

In order to validate the simulation results, for each case, the flow velocities of all outlet branches in hyperemia situation were calculated and compared with the normal physiological range of hyperemic flow velocity in coronary arteries (18), (19). The Pearson correlation coefficient (Pearson's R) between outlet cross-section area and flow velocity of each case was calculated to see if Murray's law is conformed, which indicates that a larger outlet branch has a higher flow velocity.

**2.5. Effect of MR variation on flow rate and iFR in stenotic and normal cases**

The effect of MR variation on blood flow rate and iFR was estimated by comparing the blood flow and iFR values among six situations of MR, in both the stenotic and normal cases. Flow rate was

calculated and normalized as the relative value referring to the “hyperemia” value. In each case, flow rates of all outlet branches were juxtaposed radially in a radar diagram.

## 3. Results

### 3. 1. Validation results of hyperemic blood flow velocity

Table 1 shows the blood flow velocity distribution under the reference “hyperemia” situation, respectively for each case. The inlet flow rates and velocities were within 3.7-7.5ml/s and 0.25-0.50m/s, respectively. The simulated range of flow rate covered the healthy hyperemic LMCA flow rate (approximately 4.5 ml/s) (19). According to the results of Doppler echocardiography, the peak diastolic velocity of LMCA varied from 1.16±0.28m/s to 0.29±0.12m/s in normal and stenosed LMCAs (20). Our simulation results were within this wide range. The outlet flow velocity of the four cases ranged from 0.19 to 0.49m/s, which was in accordance with the clinically measured range during hyperemic wave-free period (0.21-0.614m/s) (18). In an earlier study, the average hyperemic velocity measured by Doppler angioplasty was 0.19±0.12m/s and 0.45±0.12m/s in stenosed and normal distal segments of coronary arteries, respectively (21). Our simulation results were in accordance with existing physiological studies. For the outlets, the velocity was positively correlated with cross-sectional area (Pearson’s R overall four cases: 0.793, and >0.61 in each case).

Table 1. The inlet velocity, maximum and minimum of outlet velocities, and Pearson correlation coefficient (Pearson's R) between outlet area and velocity in each case.

| Case number | Inlet velocity (m/s) | Maximum outlet velocity (m/s) | Minimum outlet velocity (m/s) | Pearson’s R between outlet area and velocity |
|---|---|---|---|---|
| 1 (mild stenosis) | 0.25 | 0.29 | 0.33 | 0.99 |
| 2 (normal) | 0.50 | 0.38 | 0.49 | 0.62 |
| 3 (severe stenosis) | 0.24 | 0.19 | 0.30 | 0.62 |
| 4 (normal) | 0.35 | 0.23 | 0.33 | 0.91 |

### 3.2. Effect of MR variation on blood flow rate

Fig.2 shows the relative flow rate with different MR variations, in comparison with reference “hyperemic” value.

Firstly, resting situation always had the lowest flow rate (about 40% of hyperemia values) when compared with the other four situations with MR increase (h-one-1.5, h-one-2, h-branches-1.5, h-branches-2) (Fig.2).

Secondly, MR variation in a branch significantly changed its flow rate. In all the four cases, when MR of an outlet branch was doubled (in branches 1, 2, and 3 for h-branches-2, and in branch 1 for h-one-2), its relative flow rate decreased by more than 40 % (cyan and purple lines in Fig.2, compared with red lines).

Finally, MR variation in a branch did not lead to any significant effect on the flow rates of other branches without MR variation, except in Case 3 with severe stenosis (96.4% in area). In cases 1, 2, and 4, in the branches without MR variation (for h-branches-1.5 and h-branches-2: branches 4-6 in cases 1 and 2, branches 4-11 in Case 4; for h-one-1.5 and h-one-2: branches 2-6 in cases 1 and 2, branches 2-11 in Case 4), the reduce of flow rate was within 3% compared with the hyperemic value (Fig.2). Whereas, in Case 3, when MR of branch 1 was doubled (h-one-2), the flow rates of its cognate

branches increased significantly (>10% and about 8% in branches 2 and 3), resulting in the "branch steal" phenomenon.

Fig.3 illustrates the change of flow velocity in stenotic cases 1 and 3 with doubled MR (in branch 1 for h-one-2, and in branches 1-3 for h-branches-2). For both cases, the branches with doubled MR have obvious velocity changes. No significant flow change was observed in branches without MR doubling, except in h-branches-one situation of Case 3 where there were minor but observable changes of flow velocity (0.05-0.1m/s) in branches 2 and 3.

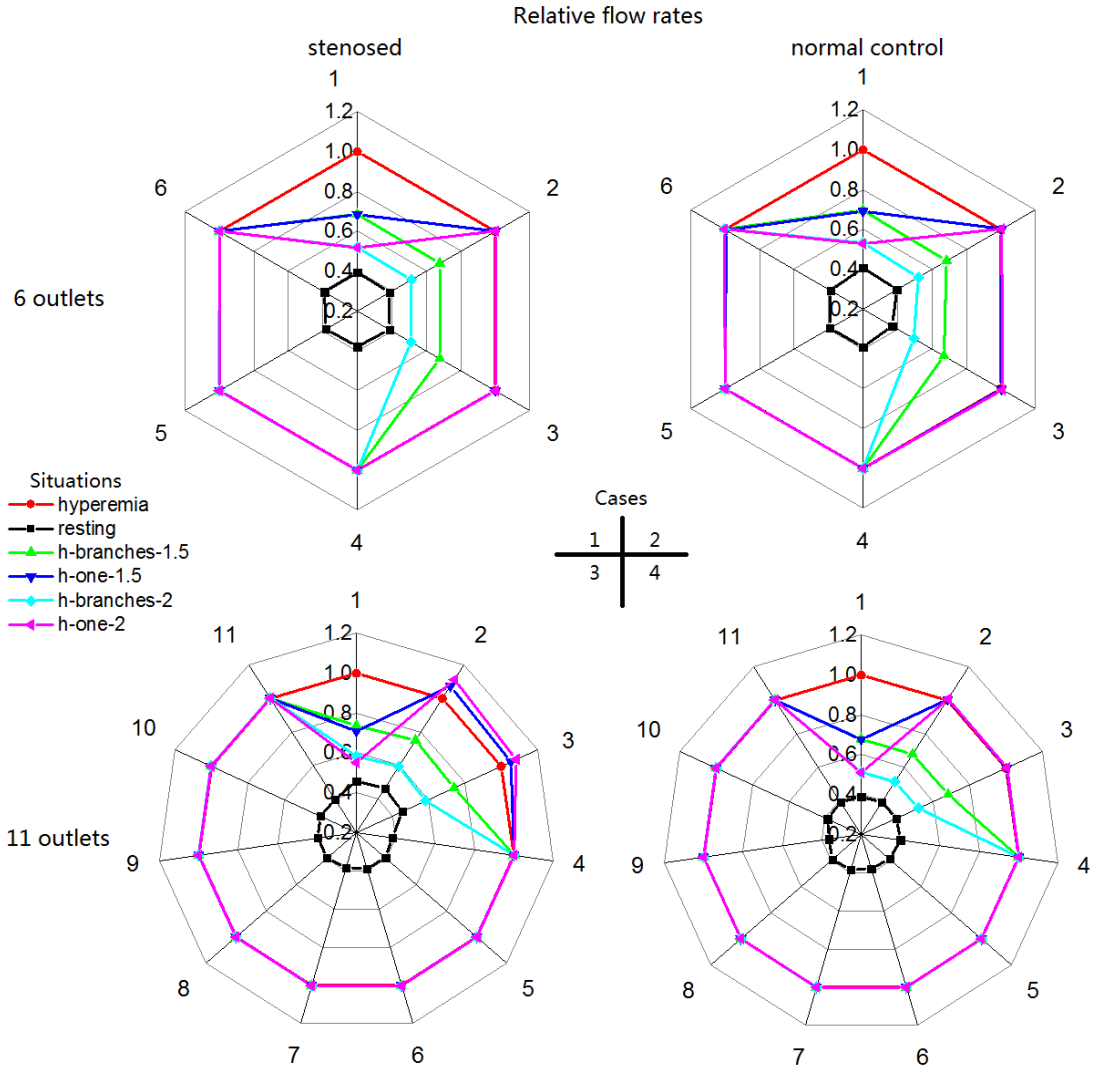


Figure 2. The relative flow rates of all outlet branches under six MR situations in four cases. The colors differentiate six MR situations. The numbers according to the radius in each subfigure indicate corresponding outlet branches in Fig.1. For each case, hyperemia is the reference situation. For an outlet branch, the flow rates in other situations are shown as relative values compared with the corresponding value in hyperemia situation.

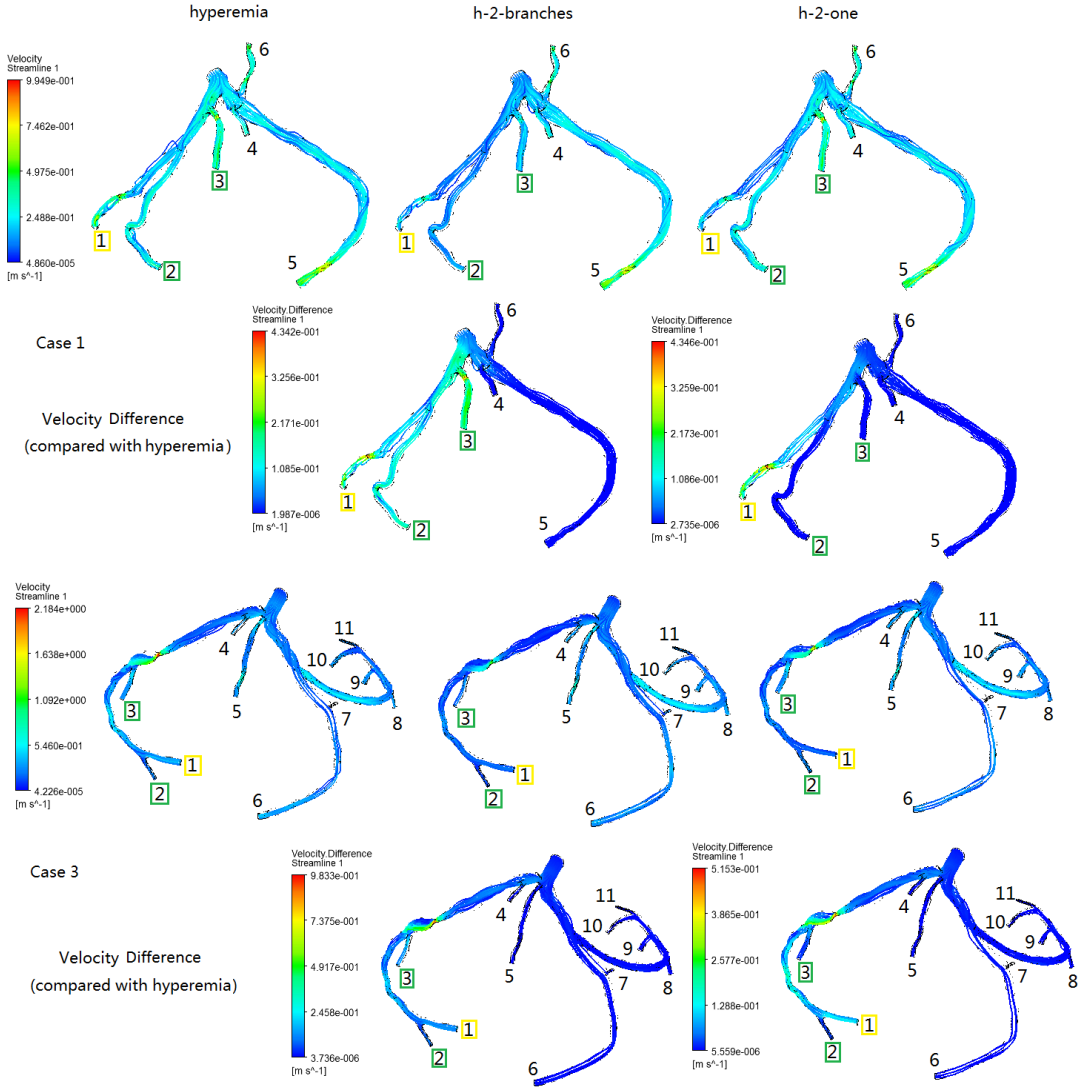


Figure 3. The velocity variations due to MR increase in cases 1 and 3. In h-2-branches situation, the MR values of branches 1, 2, and 3 (with yellow or green rectangle) were doubled. In h-2-one situation, the MR value of branch 1 (with yellow rectangle) was doubled. The second and fourth rows show the corresponding difference in velocity of h-2-branches and h-2-one situations compared to the hyperemia situation.

### 3.3. Effect of MR variation on iFR

Fig.4 illustrates the iFR values of all the outlet branches of the four cases in six different situations of MR. In normal cases 2 and 4, the difference in iFR were within $\pm 0.05$ among all situations. In mildly stenotic Case 1, the maximal iFR difference was 0.07 in branch 1, and smaller than 0.05 in the other branches. In severely stenotic Case 3, the maximum iFR difference was 0.168, 0.169, and 0.155 in branches 1, 2, and 3, respectively, and was within 0.06 in other outlets. The branches 1, 2, and 3 were distal to the severe stenosis (Fig.1), revealing the combined effects of MR and stenosis on iFR.

On the one hand, the increase of MR in a branch caused the increase of its iFR. In all the outlet branches, the resting and hyperemia (reference) situations had the highest and lowest iFR values. When MR was partially increased (in branch 1 for h-one-1.5 and h-one-2, in branches 1, 2, and 3 for h-branches-1.5 and h-branches-2), for any branch, its iFR values in these situations were between the

corresponding values in hyperemia and resting situations. On the other hand, the MR variation in a branch did not influence the iFR of the other branches without MR variation, except in Case 3 with severe stenosis (96.4% in area). In cases 1, 2, and 4, with the increase of MR in branch 1 (h-one-1.5 and h-one-2), significant increase of iFR (>0.02) was observed in branch 1 only (change of iFR<0.01, or <1% compared with hyperemia iFR in other branches). Whereas, in Case 3, the increase of MR in branch 1 (h-one-1.5 and h-one-2) resulted in significant increase of iFR (>0.05) in its cognate branches 2 and 3.

In situations h-branches-1.5 and h-branches-2, the increase of iFR was limited to branches 1, 2, and 3 in all the cases.

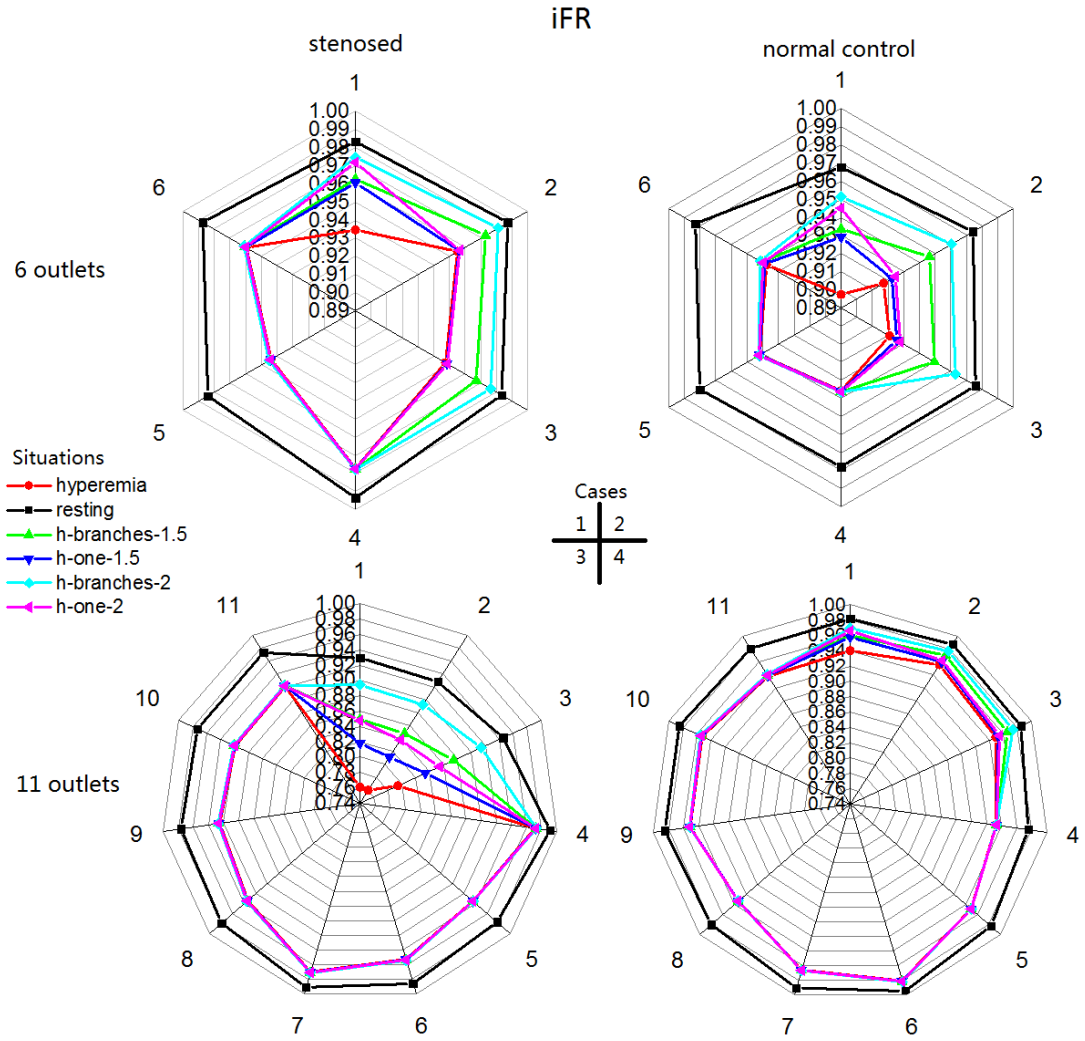


Figure 4. The variation of iFR in different MR situations. For each case, the colors differentiate the iFR values in six situations of MR. The numbers according to the radius in each subfigure indicate corresponding outlet branches in Fig.1.

## 4. Discussion

The CFD simulation showed that MR increase in an outlet branch led to the decrease in its flow rate and the increase in its iFR. In different cases, we observed a difference in the effect of MR variation in a branch on the flow rate and iFR of its cognate branches.

It has been generally accepted that the flow rate of a coronary artery is sensitive to the change of

its MR. The change of flow rate in six MR situations showed similar patterns between corresponding cases with and without stenosis in paired cases (cases 1 and 2, cases 3 and 4, in Fig.2). In cases 1 (with 74.9% stenosis in area), 2 (normal), and 4 (normal), the increase of MR in an outlet branch reduced its flow rate, without any observable effect on any other branch. However, in Case 3 (with 96.4% stenosis in area), branch steal was observed where the increase of MR in the stenotic branch resulted in the increase of flow rate in its cognate branches.

Coronary branch steal appears when a non-stenotic branch between proximal and distal stenoses shunts flow away from a parallel stenotic daughter branch (15). In this case, the blood supply of the myocardium distal to the stenotic daughter branch will be reduced, resulting in ischemia (22). Especially, in bifurcations of coronary arteries, branch steal occurs when a proximal artery and one of its distal branches are simultaneously stenotic (22). In Case 3 with 96.4% stenosis, the increase of MR in the stenotic branch has the similar effect of a distal stenosis on the blood flow. Therefore, the blood flow is supposed to be shunted away to outlets 2 and 3. However, we did not observe branch steal in stenotic Case 1. Firstly, the area ratio between outlet 1 and outlets 2 and 3 was higher in Case 3 (3.47: (2.11+0.77), in comparison with 4.47: (3.37+3.94) in Case 1). According to Murray's law, branch 1 had a much higher share of blood flow in Case 3 than in Case 1. Since MR accounts more than 80% of total flow resistance (4), the MR increase in branch 1 will cause an obvious decrease in the total flow rate of LAD in Case 3, resulting in the decrease in trans-stenotic pressure drop. Secondly, in Case 3, the severe stenosis (>90% in area) had a non-linear relationship between its trans-stenotic pressure drop and its flow rate (18). The flow resistance of the stenosis is positively related with its flow rate. With lower flow rate, the flow resistance of the stenosis was decreased, which significantly reduced the trans-stenotic pressure drop due to the non-linear relationship between flow rate and trans-stenotic pressure drop, resulting in the increase of inlet pressure in branches 2 and 3. Therefore, flow rates of branches 2 and 3 increased. In contrast, both area ratio and severity of stenosis were lower in Case 1. Therefore, increased MR at outlet 1 did not obviously elevate the pressure at inlets of branches 2 and 3, which eliminated the occurrence of branch steal phenomenon. The interaction between stenotic and microcirculatory resistances which caused branch steal phenomenon deserves further investigation.

In an outlet branch, the increase of its MR caused corresponding increase of iFR. The changes of iFR among six situations of MR were within 0.05 in most branches except for those distal to the severe stenosis in Case 3. Comparatively, FFR value is sensitive to MR variation, therefore could not independently detect the decrease in blood flow after percutaneous coronary intervention (PCI) (23), (24). The fitting results of in-vivo measurement of 255 coronary arteries indicated that, with MR doubled from 1.5 to 3 mmHg.s/cm, the increase of FFR ranged between 0.03 to 0.15 even in cases with mild stenosis (<58% in diameter, <83% in area) (3). Generally, MR variation in one branch showed limited influence on the iFR of other branches (<0.02 in cases 1, 2, and 4). Whereas, in Case 3 (Fig.4) where branch steal was observed, the doubled MR at outlet 1 (h-one-2) significantly increased the iFR (>0.06) of cognate LAD branches 2 and 3. However, in Case 3, iFR values of branches originated from LCX or other non-cognate arteries were still unaffected (changes<0.02). A study on swine models showed that, FFR values in the LAD and the LCX were independent without significant influence from each other's stenotic severity (25). Therefore, iFR could be a stable hemodynamic parameter to estimate the severity of stenosis without being affected by MR variation, but cautions should be taken in severely stenotic coronary arteries. The effect of MR variation on iFR needs further investigation especially in severely stenotic arteries.

In our study the laminar flow assumption was used in all the four cases. The peak Reynolds

number in a coronary stenosis is typically much smaller than that leading to the laminar-to-turbulent transition (approximately 2300). It has been proven that the errors due to the Newtonian and laminar approximations are negligible for stenosis severities leading to FFR values around the threshold 0.8 (26). In the tube flow, the Reynolds number is proportional to the diameter and flow velocity. Abbasian et al. calculated the Reynolds number in three coronary artery models with stenosis of 30%, about 50% and more than 60% in diameter (27). The authors did in vivo measurement of coronary flow rate and found that the Reynold number was less than 750 with maximum measured velocity (0.80 m/s) and maximum arterial diameter (3.1 mm). Similarly, Rajabi-Jaghargh simulated the blood flow in stenosed coronary arteries and found that the throat Reynolds number was 734 in the artery with 90% stenosis in area at hyperemic flow condition (28). In our simulation of the most severe stenosis in Case 3, the highest velocity was about 2.18m/s (cross-sectional average velocity: approximately 1.54 m/s) while the diameter was about 1.29 mm at the stenotic throat and 3.78mm in the normal segment distal to the stenosis. Compared with Abbasian et al.' s results, the maximum Reynolds number in our simulation was about 1762, which was much lower than the threshold of laminar-to-turbulent transition. Therefore, the laminar model is reasonable in our current study. The turbulent models could be considered in future studies focusing on post-stenotic areas where minor turbulent effect could be observed (26).

Currently there is no clinical cut-off value or normal range of MR (3). The increasing factors of MR variation (8/3, 1.5, and 2) were based on recent physiological and clinical studies, as detailed below. With chronic cardiac diseases, due to thickened small intramural arteries and narrowed lumens, hyperemic MR could increase by 40%, which leads to the MR increase factor 1.5 (9). Some pathophysiological factors such as age, diabetes, smoking habit, and hypertension, as well as the proximal coronary stenoses, could cause dysfunction in coronary microcirculation (4) where the increase of hyperemic MR could exceed 200% (3). Reversely, when stenotic lesions were released by PCI, abnormal MR could significantly decrease (23) by 29% within 2 months (29). The MR value could reflect not only the risk of ischemia but also the prognosis of PCI, therefore it is clinically important to further investigate the relationship between MR and other hemodynamic parameters (30), (31).

The limitations of this study include, first, the solid-wall assumption in CFD simulation. The myocardial contraction could compress the arterioles and capillaries, increasing MR in coronary arteries. Secondly, the static simulation was adopted in this study. In reality, the aortic pressure, MR, and geometry of coronary arteries change periodically. Therefore the conclusions are applicable exclusively to the wave-free period. Thirdly, the MR values from the literature were used. Unfortunately we didn't have the patient-specific MR values whose measurement is difficult therefore not performed in most cases. Additionally, limited by the number of cases we had, it was difficult to find the paired cases (stenosed and normal) with the same numbers of major branches and similar structures. Therefore only four cases were included in this pilot study. In future studies, the elasticity of arterial wall, the periodic fluctuation of MR, as well as the patient-specific MR values could be derived from in vivo measurement and applied in the CFD simulation of more cases covering a wider range of coronary artery stenosis to improve the accuracy of estimating the hemodynamic effect of MR variation.

**Conclusion**

This simulation study demonstrated that, firstly, the increase of MR in an outlet branch of coronary artery reduced its flow rate with minor increase in its iFR value. Secondly, MR variation in an

outlet branch has limited effect on the flow rate and iFR of other branches, except in a large branch with severe stenosis when both the flow velocity and iFR of its cognate branches could be significantly increased.

**Acknowledgments**

This work was supported by the National R&D Program for Major Research Instruments [Grant no. 61527811].

**References**

1. Morris PD, Ryan D, Morton AC, Lycett R, Lawford PV, Hose DR, et al. Virtual fractional flow reserve from coronary angiography: modeling the significance of coronary lesions: results from the VIRTU-1 (VIRTUal Fractional Flow Reserve From Coronary Angiography) study. JACC: Cardiovascular Interventions. 2013;6(2):149-57.
2. Papafaklis MI, Muramatsu T, Ishibashi Y, Lakkas LS, Nakatani S, Bourantas CV, et al. Fast virtual functional assessment of intermediate coronary lesions using routine angiographic data and blood flow simulation in humans: comparison with pressure wire-fractional flow reserve. EuroIntervention: journal of EuroPCR in collaboration with the Working Group on Interventional Cardiology of the European Society of Cardiology. 2014;10(5):574-83.
3. van de Hoef TP, Nolte F, Echavarría-Pinto M, van Lavieren MA, Damman P, Chamuleau SA, et al. Impact of hyperaemic microvascular resistance on fractional flow reserve measurements in patients with stable coronary artery disease: insights from combined stenosis and microvascular resistance assessment. Heart. 2014;100(12):951-9.
4. Guarini G, Giuseppina Capozza P, Huqi A, Morrone D, M Chilian W, Marzilli M. Microvascular function/dysfunction downstream a coronary stenosis. Current pharmaceutical design. 2013;19(13):2366-74.
5. de Waard GA, Nijjer SS, van Lavieren MA, van der Hoeven NW, Petraco R, van de Hoef TP, et al. Invasive minimal microvascular resistance is a new index to assess microcirculatory function independent of obstructive coronary artery disease. Journal of the American Heart Association. 2016;5(12):e004482.
6. Ma Y, Liu H, Hou Y, Qiao A, Hou Y, Yang Q, et al. Instantaneous wave-free ratio derived from coronary computed tomography angiography in evaluation of ischemia-causing coronary stenosis: Feasibility and initial clinical research. Medicine. 2017;96(4).
7. Matsuo H, Kawase Y, Kawamura I. FFR and iFR. Annals of Nuclear Cardiology. 2017;3(1):53-60.
8. Sejr-Hansen M, Westra J, Thim T, Christiansen EH, Eftekhari A, Kristensen SD, et al. Quantitative flow ratio for immediate assessment of nonculprit lesions in patients with ST-segment elevation myocardial infarction—An iSTEMI substudy. Catheterization and Cardiovascular Interventions. 2019;94(5):686-92.
9. Hoffman JI, Buckberg GD. The myocardial oxygen supply: demand index revisited. Journal of the American Heart Association. 2014;3(1):e000285.
10. Aetesam-ur-Rahman M, Zhao T, Giblett J, Braganza D, Clarke S, Bennett M, et al. TCT-463 Instability of Coronary Flow Velocity and Basal Microvascular Resistance does not Affect Reproducibility of iFR Post-PCI. Journal of the American College of Cardiology. 2018;72(13 Supplement):B186.
11. Morris PD, Soto DAS, Feher JF, Rafiroiu D, Lungu A, Varma S, et al. Fast virtual fractional flow

reserve based upon steady-state computational fluid dynamics analysis: results from the VIRTU-Fast study. JACC: Basic to Translational Science. 2017;2(4):434-46.
12. Morris PD, Narracott A, von Tengg-Kobligk H, Silva Soto DA, Hsiao S, Lungu A, et al. Computational fluid dynamics modelling in cardiovascular medicine. Heart. 2016;102(1):18.
13. Tesche C, De Cecco CN, Albrecht MH, Duguay TM, Bayer RR, Litwin SE, et al. Coronary CT Angiography–derived Fractional Flow Reserve. Radiology. 2017;285(1):17-33.
14. Liu H, Gong Y, Leng X, Xia L, Wong KS, Ou S, et al. Estimating current and long-term risks of coronary artery in silico by fractional flow reserve, wall shear stress and low-density lipoprotein filtration rate. Biomedical Physics & Engineering Express. 2018;4(2):025006.
15. Zhang J-M, Zhong L, Luo T, Huo Y, Tan SY, Wong ASL, et al. Numerical simulation and clinical implications of stenosis in coronary blood flow. BioMed research international. 2014;2014.
16. Cloud GC, Rajkumar C, Kooner J, Cooke J, Bulpitt CJ. Estimation of central aortic pressure by SphygmoCor® requires intra-arterial peripheral pressures. Clinical Science. 2003;105(2):219-25.
17. Huo Y, Kassab GS. Intraspecific scaling laws of vascular trees. Journal of The Royal Society Interface. 2012;9(66):190-200.
18. Nijjer SS, de Waard GA, Sen S, van de Hoef TP, Petraco R, Echavarría-Pinto M, et al. Coronary pressure and flow relationships in humans: phasic analysis of normal and pathological vessels and the implications for stenosis assessment: a report from the Iberian–Dutch–English (IDEAL) collaborators. European heart journal. 2015;37(26):2069-80.
19. Pagiatakis C, Tardif J-C, L'Allier PL, Mongrain R. A numerical investigation of the functionality of coronary bifurcation lesions with respect to lesion configuration and stenosis severity. Journal of biomechanics. 2015;48(12):3103-11.
20. Yamagishi M, Yasu T, Ohara K, Kuro M, Miyatake K. Detection of coronary blood flow associated with left main coronary artery stenosis by transesophageal doppler color flow echocardiography. Journal of the American College of Cardiology. 1991;17(1):87.
21. Ofili EO, Labovitz AJ, Kern MJ. Coronary flow velocity dynamics in normal and diseased arteries. The American Journal of Cardiology. 1993;71(14):D3-D9.
22. Frattolin J, Zarandi MM, Pagiatakis C, Bertrand OF, Mongrain R. Numerical study of stenotic side branch hemodynamics in true bifurcation lesions. Computers in biology and medicine. 2015;57:130-8.
23. Niida T, Murai T, Yonetsu T, Kanaji Y, Usui E, Matsuda J, et al. Coronary physiological assessment combining fractional flow reserve and index of microcirculatory resistance in patients undergoing elective percutaneous coronary intervention with grey zone fractional flow reserve. Catheterization and Cardiovascular Interventions. 2018.
24. Hamaya R, Kanaji Y, Usui E, Hoshino M, Murai T, Yonetsu T, et al. Improvement of Fractional Flow Reserve after Percutaneous Coronary Intervention Does Not Necessarily Indicate Increased Coronary Flow. Eur Cardiol. 2019;14(1):10-2.
25. Oh JH, Song S, Kim C, Kim J, Sup Park J, Won Lee H, et al. The influence of side branch stenosis on fractional flow reserve assessment of the main branch in a swine model. Catheterization and Cardiovascular Interventions. 2017;89(2):219-25.
26. Agujetas R, González-Fernández MR, Nogales-Asensio JM, Montanero JM. Numerical analysis of the pressure drop across highly-eccentric coronary stenoses: application to the calculation of the fractional flow reserve. BioMedical Engineering OnLine. 2018;17(1):67.
27. Abbasian M, Shams M, Valizadeh Z, Moshfegh A, Javadzadegan A, Cheng S. Effects of different non-Newtonian models on unsteady blood flow hemodynamics in patient-specific arterial models

with in-vivo validation. Computer Methods and Programs in Biomedicine. 2020;186:105185.
28. Rajabi-Jaghargh E, Kolli KK, Back LH, Banerjee RK. Effect of guidewire on contribution of loss due to momentum change and viscous loss to the translesional pressure drop across coronary artery stenosis: An analytical approach. BioMedical Engineering OnLine. 2011;10(1):51.
29. Keulards Daniëlle CJ, Karamasis Grigoris V, Alsanjari O, Demandt Jesse PA, van't Veer M, Zelis Jo M, et al. Recovery of Absolute Coronary Blood Flow and Microvascular Resistance After Chronic Total Occlusion Percutaneous Coronary Intervention: An Exploratory Study. Journal of the American Heart Association. 2020;9(9):e015669.
30. Murai T, Kanaji Y, Yonetsu T, Lee T, Matsuda J, Usui E, et al. Preprocedural fractional flow reserve and microvascular resistance predict increased hyperaemic coronary flow after elective percutaneous coronary intervention. Catheterization and Cardiovascular Interventions. 2017;89(2):233-42.
31. De Maria GL, Cuculi F, Patel N, Dawkins S, Fahrni G, Kassimis G, et al. How does coronary stent implantation impact on the status of the microcirculation during primary percutaneous coronary intervention in patients with ST-elevation myocardial infarction? European heart journal. 2015;36(45):3165-77.